View metadata, citation and similar papers at core.ac.uk

brought to you by CORE

provided by NASA Technical Reports Server

NASA TECHNICAL NOTE

NASA TN D-3017

NASA TN D-3017

TECH LIBRARY KAFB, NM

0079901

LOAN COPY: RETURN TO
AFWL (WLIL-2)
KIRTLAND AFB, N MEX

PRESSURE AND CONVECTIVE HEAT-TRANSFER MEASUREMENTS IN A SHOCK TUNNEL USING SEVERAL TEST GASES

by Joseph G. Marvin and Clifford M. Akin

Ames Research Center
Moffett Field, Calif.

NATIONAL AERONAUTICS AND SPACE ADMINISTRATION • WASHINGTON, D. C. • SEPTEMBER 1965

TECH LIBRARY KAFB, NM
0079901
NASA TN D-3017

PRESSURE AND CONVECTIVE HEAT-TRANSFER MEASUREMENTS IN A SHOCK TUNNEL USING SEVERAL TEST GASES

By Joseph G. Marvin and Clifford M. Akin

Ames Research Center
Moffett Field, Calif.

NATIONAL AERONAUTICS AND SPACE ADMINISTRATION

For sale by the Clearinghouse for Federal Scientific and Technical Information
Springfield, Virginia 22151 – Price $2.00

PRESSURE AND CONVECTIVE HEAT-TRANSFER MEASUREMENTS IN A SHOCK TUNNEL USING SEVERAL TEST GASES

By Joseph G. Marvin and Clifford M. Akin
Ames Research Center

SUMMARY

Pressures on a hemisphere-cylinder, and convective heat transfer on a hemisphere-cylinder, a blunted 30° cone, and the afterbody of a capsule-type shape were measured in air, nitrogen, carbon dioxide, and argon. The tests were performed in a combustion-driven shock tunnel at enthalpies from 3300 to 5400 Btu/lb, depending on the test gas.

The pressure distributions on a hemisphere-cylinder did not differ significantly in the various test gases. This was influenced by nonequilibrium effects which occurred when some of the gases passed over the model.

The stagnation-point heat-transfer data compared reasonably well with theory. On the basis of equivalent total enthalpy, the heat-transfer rate in argon was approximately 30 percent higher than that of the other gases. The heating-rate distributions on all the configurations were not influenced significantly when the test gas was changed. The distribution of heating on the hemisphere-cylinder was adequately predicted by theory using measured surface pressures.

INTRODUCTION

The convective heat transfer to a body flying in gases different from air is of interest to the designer of probes entering planetary atmospheres. Within the last few years several analytical and experimental studies have been undertaken to determine convective heat transfer in gases present in these atmospheres. See, for example, references 1 to 7. It was found in reference 3 that the heating-rate distribution in air, nitrogen, hydrogen, carbon dioxide, and argon depends mainly on the inviscid flow as reflected in the surface-pressure distribution and the boundary-layer-edge velocity. Little or no experimental data at sufficiently high enthalpies were available, except for air, to verify this conclusion; therefore, an experimental program was undertaken to obtain heating-rate distribution data on simple configurations with different surface-pressure distributions.

It is the purpose of this report to present experimental surface pressure and heating-rate distribution data obtained in air, nitrogen, carbon dioxide,

and argon at stagnation enthalpies sufficiently high to cause real-gas effects in the flow field around the models. These results are compared with one another and with theory.

SYMBOLS

C	constant in equation (4)
$\overline{C}$	constant in equation (3)
$g'(0)$	wall enthalpy gradient normal to the wall in a transformed coordinate system
g	normalized total enthalpy, H/H_{e_o}
H	total enthalpy
m	exponent describing dependence of heating-rate ratio on pressure ratio
n	shape parameter $n = 1$ for axisymmetric bodies and $n = 0$ for two-dimensional bodies
$\overline{N}$	velocity exponent in equation (3)
p	pressure
Pr	Prandtl number
q_w	wall heat-transfer rate
r	body coordinate (see fig. 2)
R	body nose radius
R_b	maximum radius of capsule configuration (see fig. 2)
t	time
u	velocity in streamwise direction
$\overline{U}$	average velocity along stagnation streamline
x	distance along the body surface in the streamwise direction measured from the stagnation point
X_N	ratio of the number of nitrogen atoms to the total number of available nitrogen atoms
X_O	ratio of the number of oxygen atoms to the total number of available oxygen atoms

X_O^*, X_N^*	equilibrium atom fractions based on the nonequilibrium temperature
Z	ratio of number of moles of gas to original number of cold moles
α	degree of ionization
Δ	shock standoff distance
μ	viscosity
ρ	density

Subscripts

e	outer edge of the boundary-layer value
o	stagnation-point value
t	total stream condition obtained by isentropically bringing the stream to rest
w	wall value
2	condition behind a normal shock
∞	free-stream value

APPARATUS AND TEST CONDITIONS

Facility and Instrumentation

The tests were performed in the Ames 1-Foot Shock Tunnel. A schematic drawing of the essential components of this facility is shown in figure 1. A complete description of the components and operating conditions using air as the test gas is presented in references 8 and 9. Briefly, this facility uses a combustion-driven shock wave reflected off the end wall of the driven section to compress the test gas to a high enthalpy and pressure. This gas is then expanded through a nozzle and over the test model. A 20°-included-angle conical nozzle with a 1-foot exit diameter and a 0.2-inch throat diameter was used for all tests.

Instrumentation for the 1-foot shock tunnel is also described in references 8 and 9. The incident shock-wave velocity is determined from five ionization probes spaced along the driven section, and the stagnation pressure is determined with quartz-crystal transducers with response times sufficiently rapid to measure the incident and reflected shock pressures. Use of gases other than air produced no adverse effects on this instrumentation.

Test Conditions

Prior to the present investigation, the 1-foot shock tunnel had used only air as the test gas, and tunnel calibration data were lacking for other gases. The following table lists the nominal tailored-operating test conditions for air and those that were estimated for the other gases.

Gas	H_t, Btu/lb	p_t, atm	u_∞, ft/sec	p_o, atm	Z_{e_o}, equil	α_{e_o}, equil
Air	4500	285	13,000	0.150	1.23	0
N_2	5000	285	14,900	.146	1.2	0
CO_2	5400	285	12,000	.140	1.75	0
A	3250	285	12,700	.150	---	.06
	5130	285	16,000	.117	---	.15

The estimated gas purity was 99.4 percent by volume. Test times were approximately 25 milliseconds in all gases.

The stagnation enthalpy was obtained by solving the conservation equations across the incident-normal and reflected-normal shocks. Initial driven-section pressure and incident shock velocity were measured and the appropriate thermodynamic data were calculated by H. Bailey of Ames. Since the measured total pressure was higher than the calculated reflected shock pressure, the final stagnation enthalpy was obtained by assuming isentropic compression from the calculated pressure to the measured pressure. This usually resulted in an increase in total enthalpy of approximately 10 percent.

Measurements of test-section static pressure in air and carbon dioxide indicated the test streams in these gases were frozen. For air, a freeze Mach number and test-section velocity were determined by matching test-section pitot- and static-pressure measurements with those calculated in reference 10 for the stagnation enthalpy and the effective area ratio, obtained from a mass-flow-probe measurement. The mass-flow probe was similar to the one described in reference 11. For carbon dioxide, information similar to that in reference 10 was not available so the gas was assumed to be fully excited vibrationally, and chemically frozen at the stagnation conditions of pressure and enthalpy. The effective area ratio determined for air was then used in estimating the test-section velocity. For nitrogen the free-stream velocity was obtained from a nonequilibrium nozzle calculation using the air effective-area ratio. The computer program for this calculation is described in reference 12. For these test gases, the effect of free-stream dissociation on the test results was assumed to be negligible. For argon the free-stream velocity was estimated from the air effective area ratio with the assumption of thermochemical equilibrium through the nozzle. This was a reasonable assumption since the high-enthalpy argon in the driven section was only electronically excited, and the spontaneous decay from this state takes place very rapidly compared to the flow time.

Models and Instrumentation

Three configurations were used for these tests (see fig. 2). The nose sections were spherical, followed by either conical or cylindrical afterbodies. Configuration A was a hemisphere-cylinder approximately 3 diameters long. Configuration B was a spherically-blunted 30° half-angle cone. Configuration C was a spherically-blunted capsule shape with a conical afterbody.

A pressure model was constructed for configuration A only. It was made of stainless steel and instrumented with capacitance-type pressure transducers flush-mounted to the inside of the model wall. Orifice openings 0.09 inch in diameter on the model surface exposed the measuring side of the transducer to the surface pressure. The transducers had a diaphragm separating the measuring and reference sides. The capacitance change of a gap on the reference side gave a measure of the pressure when the diaphragm deflected. The transducer range was from 0 to 5 psia.

A thin-walled, heat-transfer model of configuration A was made from electroformed copper. The hemispherical nose was 0.015 inch thick and the cylindrical afterbody was 0.010 inch thick. Three techniques were used to install thermocouples because of the difficulty of spot-welding to copper. Along one meridian plane, single No. 40 gage constantan wires were installed in holes drilled through the skin and then silver soldered into place. (Information in the NBS standard monograph (March 1962) on thermocouple materials and the ASTM spec B-3-45 for copper showed that the copper model shell was suitable for thermocouple use.) A common copper wire was silver soldered to the rear of the model, thus completing a copper-constantan junction. Diametrically opposite the single wire junctions, a second row of copper-constantan thermocouples was installed in the same manner as the single constantan wire. Finally, two copper-constantan thermocouples were spot-welded near the rear of the copper shell. Measurements of heating rates with these three thermocouple installations agreed closely.

For configuration B the model was electroformed from pure nickel to a wall thickness of 0.010 inch. For configuration C the nose was thick copper, and the afterbody was made of 301 stainless steel with a 0.010-inch wall thickness. Both of these models were instrumented with No. 36 gage chromel-constantan thermocouples spot-welded to the inside of the model skin. These models were on hand at the time the investigation was started.

Some of the stagnation-point heat-transfer data presented herein were measured on a 1-inch-diameter hemisphere. This hemisphere was made of copper with a wall thickness of 0.010 inch and was instrumented with a chromel-constantan thermocouple silver soldered to the inner surface.

Test Technique

Before and after each pressure test a calibration of the transducers was performed. The measuring side was exposed to atmospheric pressure, and a vacuum was drawn on the reference side in finite increments. The calibrations

before and after the test runs showed excellent agreement. During the test runs, the reference pressure in the cell was maintained at 25 microns, and the capacitance change was recorded on a high-speed oscillograph. The estimated error was ±10 percent of the measured pressure.

The heat-transfer data were obtained by determining the temperature response of the thin-shelled models described above. Thermocouple outputs were amplified and recorded on a high-speed oscillograph (160 inches of paper per second). The oscillograph deflections were curve fitted as a function of time and converted to heat-transfer rates by an electronic computing machine. The estimated maximum error was ±10 percent in the heat-transfer rate.

RESULTS AND DISCUSSION

Pressures

The heating rate and heating-rate distribution depend strongly on the inviscid flow over a body. Therefore, the discussion of the test results begins with the pressure distribution, since it essentially describes the inviscid flow.

Pressure measurements.- Pressures were measured along the surface of the hemisphere-cylinder in the various test gases. These data are presented in figure 3. The model surface pressure, normalized by the measured stagnation-point pressure, is plotted against the dimensionless distance along the body surface, x/R. (The shoulder-location data for nitrogen and argon are not plotted because the capacitance cell in the model at this location failed prior to runs in those gases.) The pressure distributions in the various gases are nearly the same. Such a result was expected over the region of the forebody where modified Newtonian theory should apply but not over the cylindrical afterbody in light of the differing test conditions. For example, calculations using the blunt body and method of characteristics programs described in reference 13 have shown that afterbody pressures in CO_2 could be as much as 50 percent lower than in air, given the same free-stream density and velocity and with thermochemical equilibrium assumed. Therefore, it is useful to investigate these results in more detail.

As will be shown, it is believed that the reason for the good agreement of the experimental pressure distributions in figure 3 is that for the tests in air, nitrogen, and carbon dioxide, the chemical composition of the test gas froze as the gas expanded over the model. This would result in afterbody pressure ratios which would be about the same for these gases because the frozen value of the isentropic exponent was about the same. Furthermore, the pressure ratio levels of these gases are fortuitously about the same as those for argon.

In order to demonstrate the latter point, a perfect-gas air and an equilibrium-argon calculation of p/p_o using the programs described in reference 13 for uniform free-stream flow are compared in figure 3. (The perfect-gas air calculation for the present test conditions is very similar to that

obtained by freezing the flow along the streamlines in the shock layer. See reference 14, figure 59.) The theory predicts only minor differences in pressure ratio for the present air and argon test conditions, although the predicted values are considerably higher than the data. This difference between the predicted and measured pressures is attributed mainly to conical flow in the nozzle which causes the measured surface pressures to be lower than those obtained in uniform flow; for example, see references 15 and 16. An estimate of this effect was made by modifying the programs described in reference 13 to account for conical source flow in the free stream. The dashed lines in figure 3 represent the maximum expected effect of conical flow. The agreement with the data is somewhat better and the observed differences in air and argon pressure are predicted. Corrections to the data for this effect are not made herein, since the main objective is to study the heat transfer which is obtained in the same conical flow environment.

Nonequilibrium consideration.- In order to demonstrate why it was believed that the flow over the model was out of equilibrium for some of the tests, a nonequilibrium streamtube calculation was carried out. This was done for air only, but the conclusions regarding freezing of the chemical composition of the gas are believed applicable to the nitrogen and carbon dioxide tests. The nonequilibrium program used here is described in reference 12. Visualize a streamtube that is close to the stagnation streamtube and that is very near the outer edge of the boundary layer (see fig. 4). To start the calculation, initial values of velocity, density, and pressure were chosen, and the measured surface pressures were used to continue the calculations along the streamtube. A finite value of initial velocity was required to start the calculation, but as mentioned later, its magnitude did not influence the chemical composition away from the stagnation point. Calculations were made with two different assumptions regarding the initial state of the gas. Case I assumed the initial density and velocity to be that behind a normal shock for no chemical reactions but for equilibrium vibrational excitation. Case II assumed the initial density and velocity as the thermochemical equilibrium values behind a normal shock. From these initial conditions, calculations were started at $x = 0$, and the flow was expanded and allowed to dissociate and recombine according to the governing chemical rate processes. The results should give a qualitative representation of the real-gas flow over the test model. No free-stream dissociation was considered in this analysis as its effect on the results is considered to be small.

The results are demonstrated in figure 4 by plotting the number fraction of the species against x/R. (The calculations were started at $x = 0$; therefore, the initial standoff distance is excluded which makes the estimates somewhat conservative as regards chemical freezing.) The fractions X_O and X_N represent the number of oxygen and nitrogen atoms normalized by the total number of available oxygen and nitrogen atoms. Also shown are the equilibrium fractions X_O^* and X_N^* which are based on the local nonequilibrium temperature and pressure; for example, when X_O and X_O^* are equal, the oxygen is considered to be in thermochemical equilibrium. For case I dissociation of O_2 and N_2 takes place rapidly, that is, X_O and X_N reach X_O^* and X_N^* at $x/r \approx 0.8$. From this point, no measurable recombination of oxygen atoms occurs, and the composition of O is frozen along the rest of the streamtube

distance whereas the N recombines to form N_2 rapidly enough to maintain itself in equilibrium. Similar results are found for case II (fig. 4), which starts with the gas in the thermochemical equilibrium. Here the chemical composition freezes sooner than for case I. The difference in initial values of X_O^* and X_N^* between cases I and II results from the different assumptions regarding the initial state of the gas.

Other calculations, with much smaller initial velocities, show the same trends exhibited by cases I and II, and all of these show that the chemical composition of oxygen was frozen for $x/R > 0.8$. These results suggest that the inviscid air flow around this body is not in thermochemical equilibrium. For the two other gases, nitrogen, and especially carbon dioxide, the same conclusion is believed to apply.

Before leaving the subject of nonequilibrium flow, case I can be used to infer something about the condition of the inviscid flow in the vicinity of the stagnation point. The flow time for a particle moving along a streamline in the vicinity of the stagnation streamline from the shock to the body can be approximated by $t = \Delta/\bar{U}$, where Δ is the shock standoff distance, and $\bar{U}$ is the average velocity along the streamline which to a good approximation is $u_2/2$. Then, with the approximation, $\Delta/R \approx \rho_\infty/\rho_2 = u_2/u_\infty$, the following time is obtained: $t = 2R/u_\infty$. (This is often used as the approximate dwell time of a fluid particle in the vicinity of the stagnation point; for example, see references 17 and 18.) This time was converted to an equivalent distance, as shown in figure 4. The result shows that the gas near the stagnation point is very close to its equilibrium chemical composition. This is also concluded to be the case for the nitrogen tests, but no conclusion regarding the carbon dioxide tests can be inferred.

Heat Transfer

Before examining the heat-transfer data in detail, the equations for computing the heat transfer to a body are reviewed. For further details see reference 3.

The equation governing stagnation-point heat transfer can be written as

$$q_{w_O} = \frac{H_{e_O}}{Pr_w}\sqrt{2^n(\rho_w\mu_w)_O}\sqrt[4]{\frac{2}{R^2}\left(\frac{p_O}{\rho_{e_O}}\right)}\,[g_O'(0)] \tag{1}$$

Here, the well-known Newtonian value for the stagnation-point velocity gradient has been assumed. The heat transfer at other points on an isothermal surface, with local similarity assumed can be expressed in terms of the stagnation-point heating rate by

$$\frac{q_w}{q_{w_O}} = \frac{r^n\left(\frac{p}{p_O}\right)\left(\frac{u_e}{u_\infty}\right)}{\sqrt{2^{n+1}\int_O^x\left(\frac{p}{p_O}\right)\left(\frac{u_e}{u_\infty}\right)r^{2n}\,dx}\sqrt[4]{\frac{2}{u_\infty^2R^2}\left(\frac{p_O}{\rho_{e_O}}\right)}}\left[\frac{g'(0)}{g_O'(0)}\right] \tag{2}$$

Equations (1) and (2) consist of the product of inviscid and viscous quantities. The inviscid quantities require knowledge of the pressures discussed above. The viscous quantities, $g'(0)$ and $g_o'(0)$, require the appropriate solution to the boundary-layer equations which are implicitly related to the inviscid flow through the local surface pressure and pressure gradient. An extensive study of the latter quantities for several real gases in thermochemical equilibrium is presented in reference 3. Their results show that equation (1), for the gases considered herein, can be written as

$$q_{w_o} = \overline{C} \sqrt{\frac{p_o}{R}} \left(\frac{u_\infty}{10{,}000} \right)^{\overline{N}} \left(1 - \frac{H_w}{H_{e_o}} \right) \tag{3}$$

and the viscous terms in equation (2) (for axisymmetric flow) as

$$\frac{g'(0)}{g_o'(0)} = \left(1 + C \left\{ \frac{2\left[\int_o^x \left(\frac{p}{p_o} \right) \left(\frac{u_e}{u_\infty} \right) r^{2n} \, dx \right] \frac{d}{dx} \left(\frac{u_e}{u_\infty} \right)}{\left(\frac{u_e}{u_\infty} \right)^2 \left(\frac{p}{p_o} \right) r^{2n}} \right\} \right)^{1/2} \Bigg/ \left(1 + 0.707\, C \right) \tag{4}$$

where the various constants are listed in table I. Furthermore, for a practical range of local velocity gradients, $g'(0)/g_o'(0)$ does not depart significantly from unity. These conclusions also apply to frozen boundary layers on bodies with catalytic walls. See, for example, references 17 and 19.

It is informative now to present the heat-transfer data and to compare them with the above equations. In all comparisons with theory, it is assumed that the gas within the boundary layer is in equilibrium.

Stagnation-point heat transfer.- During the heating-rate distribution tests and during some preliminary calibration tests, the stagnation-point heat transfer to 1- and 2-inch-diameter hemispherical noses was measured. These data are plotted in figure 5 and compared with equation (3) and with some shock-tube test data. Generally, the data agree reasonably well with the other test data and equation (3). The theory predicts that argon has the highest heating rate followed in order by carbon dioxide, air, and nitrogen. The present data (with the possible exception of carbon dioxide) substantiate this. For both argon and carbon dioxide the data are consistently below theory. Part of the reason for this is the uncertainty in total test stream conditions for these two gases. For example, Bailey's thermodynamic data lead to the uncertainty in total enthalpy for carbon dioxide at high pressures (see, e.g., ref. 20), represented by the horizontal bar in figure 5(c). Further discussion regarding other factors, such as nonequilibrium stagnation-point heating, are not within the scope of the present investigation.

Heating-rate distribution.- The primary purpose of this investigation was to provide heating-rate distribution data in several gases and to compare these with one another and with theory. These data are presented next.

The heating-rate distribution for the hemisphere-cylinder is presented in figures 6(a) to 6(d) for each of the four gases, and all of the data are plotted in figure 6(e) for comparison. The local heating rate, normalized by the measured stagnation-point heating rate, is plotted against x/R. Generally, over the whole configuration, the heating rates follow the same trends exhibited by the pressures. In figure 6(e) it is observed that air has the highest heating-rate ratio at any x/R, the other gases grouping somewhat below, but essentially in the same order as the pressures.

At this point, it is logical to inquire about the comparison of these data with equation (2). In order to evaluate equation (2) the pressure ratio (a measured quantity), the velocity ratio u_e/u_∞, and the enthalpy-gradient ratio are required. The enthalpy-gradient ratio was obtained from numerical solutions to the boundary-layer equations. This ratio generally ranged between 1.0 and 0.90 over the body. The velocity ratio was obtained by making various assumptions regarding the inviscid gas state (i.e., equilibrium or frozen), except for argon which was considered to be in thermochemical equilibrium. The solid lines in figures 6 represent equation (2) for the assumption of an equilibrium isentropic expansion of the gas from the stagnation point around the body. The agreement with the data on the forebody is very good, but the theory overpredicts the level of the heating somewhat on the afterbody, especially following the shoulder. The dashed curve, which compares more favorably with the air, nitrogen, and carbon dioxide data, was obtained by freezing the chemical composition and vibrational state of these gases at their respective equilibrium values at the sonic point on the forebody and by using the resulting u_e/u_∞ in equation (2). (This is an appropriate assumption in light of the previous discussion on nonequilibrium considerations.) This lowers the level of equation (2), bringing the data and theory into better agreement, although the afterbody data are consistently lower than equation (2). It is noteworthy that the heating-rate distribution is not altered significantly by the assumption used to calculate u_e/u_∞. In this regard, it was also found that the heating-rate distribution computed by equation (2) was not altered significantly if u_e/u_∞ was calculated by assuming frozen flow at the boundary-layer edge from the stagnation point around the body. Evidently, equation (2) depends mainly on the pressure ratio itself, at least for the range of enthalpy considered in these tests.

With this result in mind, it is informative to plot the measured pressure ratios against the measured heating-rate ratios as in figure 7. (A curve was "faired" through the measured pressures to obtain pressure data at x/R locations corresponding to those for the heat transfer.) Also plotted in figure 7 are some unpublished helium data and some air data from references 14 and 21. The solid lines represent equations of the form $q_w/q_{w_o} = (p/p_o)^m$. The data generally lie between the curves for $m = 0.8$ and 1.0. Over the forebody m assumes values between 0.8 and 0.9 while over the afterbody, values for m

are between 0.9 and 1.0. This result shows the strong dependence of the heating-rate ratio on the pressure ratio and is useful for obtaining quick estimates of the heating-rate ratio.

The heating-rate distribution on the 30° blunted cone in air and carbon dioxide is presented in figure 8. No significant differences are observed in the heating-rate ratios for these two gases at comparable x/R locations. Although there were no accompanying pressure-distribution data obtained for this configuration, it is instructive to see whether or not equation (2) predicts the observed results. Modified Newtonian theory was used to obtain the pressures. This will give a fairly good approximation to the actual pressure, but will not predict the overexpansion of the pressure downstream of the spherical nose nor the expected small reduction in surface pressure due to conical nozzle-flow effects. With this approximation, equation (2) shows a somewhat higher heating rate on the conical afterbody for air than for carbon dioxide when the flow is assumed to be in equilibrium. If the inviscid flow is assumed to be frozen on the conical afterbody, as suggested by results from figure 4, then equation (2) would predict essentially the same heating-rate ratios as for equilibrium.

Heating-rate data on a blunted capsule-type configuration with a conical afterbody were also obtained. This type of configuration develops separated flow over the entire afterbody at low angles of attack and attached flow on the windward side at higher angles of attack. Figure 9 shows these results. In this figure the ratio of q_w/q_{w_o} for carbon dioxide to the corresponding ratio in air is plotted against x/R_b for two angles of attack representing separated and attached afterbody flows. The separated afterbody heating-rate ratio in carbon dioxide is higher than that of air, while for attached flow it appears somewhat lower. The reasons for this are not clearly understood. However, the observed differences between carbon dioxide and air are not significant, but the fact that the data agree reasonably well with one another may be a result of nonequilibrium expansion of the flow around the small corner radius.

CONCLUSIONS

Pressure and heat-transfer measurements on several simple configurations in air, nitrogen, carbon dioxide, and argon at enthalpies from 3300 to 5400 Btu/lb resulted in the following conclusions:

1. The pressure distributions on a hemisphere-cylinder did not differ significantly in the various test gases. This was probably influenced by the frozen chemical composition of some of the gases as they passed over the body. This was verified for the air tests by a nonequilibrium streamtube calculation.

2. The measured stagnation-point heating rates compared adequately with theory. Based on the same total enthalpy, the results showed that the heating rate in argon was about 30 percent higher than that for the other gases.

3. The heating-rate distributions on the various configurations were not significantly affected by changing the test gas. Theory, using measured pressures on a hemisphere cylinder and estimated pressures on a 30° blunted cone, adequately predicted the observed results.

Ames Research Center
National Aeronautics and Space Administration
Moffett Field, Calif., June 25, 1965

REFERENCES

1. Hoshisaki, H.: Heat Transfer in Planetary Atmospheres at Super-Satellite Speeds. Am. Rocket Soc. Paper 2173-61, presented at the ARS Space Flight Report to the Nation, New York, Oct. 9-15, 1961, ARS J., vol. 32, no. 10, Oct. 1962, pp. 1544-52.

2. Scala, S. M.; and Gilbert, L. M.: Theory of Hypersonic Laminar Stagnation Region Heat Transfer in Dissociating Gases. R63SD40, Gen. Elec. Space Sci. Lab., Apr. 1963.

3. Marvin, Joseph G.; and Deiwert, George S.: Convective Heat Transfer in Planetary Gases. NASA TR R-224, 1965.

4. Rutowski, R. W.; and Chan, K. K.: Shock Tube Experiments Simulating Entry Into Planetary Atmospheres. LMSD 288139, Lockheed Missiles and Space Co., Jan. 1960.

5. Nerem, Robert M.; and Morgan, C. Joe; and Graber, Bruce C.: Hypervelocity Stagnation Point Heat Transfer in a Carbon Dioxide Atmosphere. AIAA J., vol. 1, no. 9, Sept. 1963, pp. 2173-2175.

6. Gruszczynski, J. S.; and Warren, W. R.: Measurements of Hypervelocity Stagnation Point Heat Transfer in Simulated Planetary Atmospheres. R63SD29, Gen. Elec. Space Sci. Lab., Mar. 1963.

7. Collins, Daniel J.: Convective Heat Transfer in Planetary Atmospheres. J. P. L. Tech. Rep. 32-629, July 1, 1964.

8. Cunningham, B. E.; and Kraus, S.: A 1-Foot Hypervelocity Shock Tunnel in Which High-Enthalpy, Real-Gas Air Flows Can Be Generated With Flow Times of About 180 Milliseconds. NASA TN D-1428, 1962.

9. Loubsky, W. J.; Hiers, R. S.; and Stewart, D. A.: Performance of a Combustion Driven Shock Tunnel With Application to the Taylored Interface Operating Conditions. Paper presented at Third Conf. on Performance of High Temperature Systems, Pasadena, Calif., Dec. 7-9, 1964.

10. Yoshikawa, K. K.; and Katzen, E. D.: Charts for Air-Flow Properties in Equilibrium and Frozen Flows in Hypervelocity Nozzles. NASA TN D-693, 1961.

11. Brown, Alan C.; Smith, C. Edward, Jr.; Kramer, Raymond L.; and McAdams, Edward E., Jr.: The Use of Mass-Flow and Total-Enthalpy Probes in Supersonic Flow. Tech. Rep. B-07-64-1, Lockheed Missiles and Space Co., Sept. 1964.

12. Reinhardt, Walter A.; and Baldwin, Barrett S., Jr.: A Model for Chemically Reacting Nitrogen-Oxygen Mixtures With Application to Nonequilibrium Air Flow. NASA TN D-

13. Inouye, Mamoru; Rakich, John V.; and Lomax, Harvard: A Description of Numerial Methods and Computer Programs for Two-Dimensional and Axisymmetric Supersonic Flow Over Blunt-Nosed and Flared Bodies. NASA TN

14. Curtis, J. T.; Burke, A. F.; and Hayman, R. A.: An Analytical and Experimental Study of the Ionized Flow Field About a Hemisphere Cylinder and Its Effect on the Radiation Pattern of a Slot Antenna. CAL Rep. AFCRL 63-339, Aug. 1963.

15. Baradell, D. L.; and Bertram, M. H.: The Blunt Plate in Hypersonic Flow. NASA TN D-408, 1960.

16. Hall, Gordon: Effects of Ambient Nonuniformities in Flow Over Hypersonic Test Bodies. CAL Rep. 128, Aug. 1963.

17. Fay, Jay; and Riddell, Frank R.: Stagnation Point Heat Transfer in Dissociated Air. Res. Note 18, Avco Res. Lab., June 1956.

18. Hartunian, R. A.; and Thompson, W. P.: Nonequilibrium Stagnation Point Heat Transfer Including Surface Catalysis. AIAA Conf. on Physics of Entry Into Planetary Atmospheres, Aug. 26-28, 1963.

19. Kemp, Nelson H.; Rose, Peter H.; and Detra, Ralph W.: Laminar Heat Transfer Around Blunt Bodies in Dissociated Air. Res. Rep. 15, Avco Res. Lab., Everett, Mass., 1958. Also J. Aerospace Sci., vol. 26, no. 7, July 1959, pp. 421-30.

20. Bailey, Harry E.: Equilibrium Thermodynamic Properties of Carbon Dioxide. NASA SP 3014, 1965.

21. Boison, Christopher J.: Experimental Investigation of the Hemisphere-Cylinder at Hypervelocities in Air. AEDC TR-58-20, Nov. 1958.

TABLE I.- COEFFICIENTS IN HEAT-TRANSFER EQUATIONS

Gas	$\overline{C}$, $\frac{\text{Btu}}{\text{sec ft}^{3/2} \text{ atm}^{1/2}}$	$\overline{N}$	C
Air	86.9	1.99	0.096
N_2	78.8	2.03	.12
CO_2	90.4	2.04	.10
A	115.8	2.14	.10

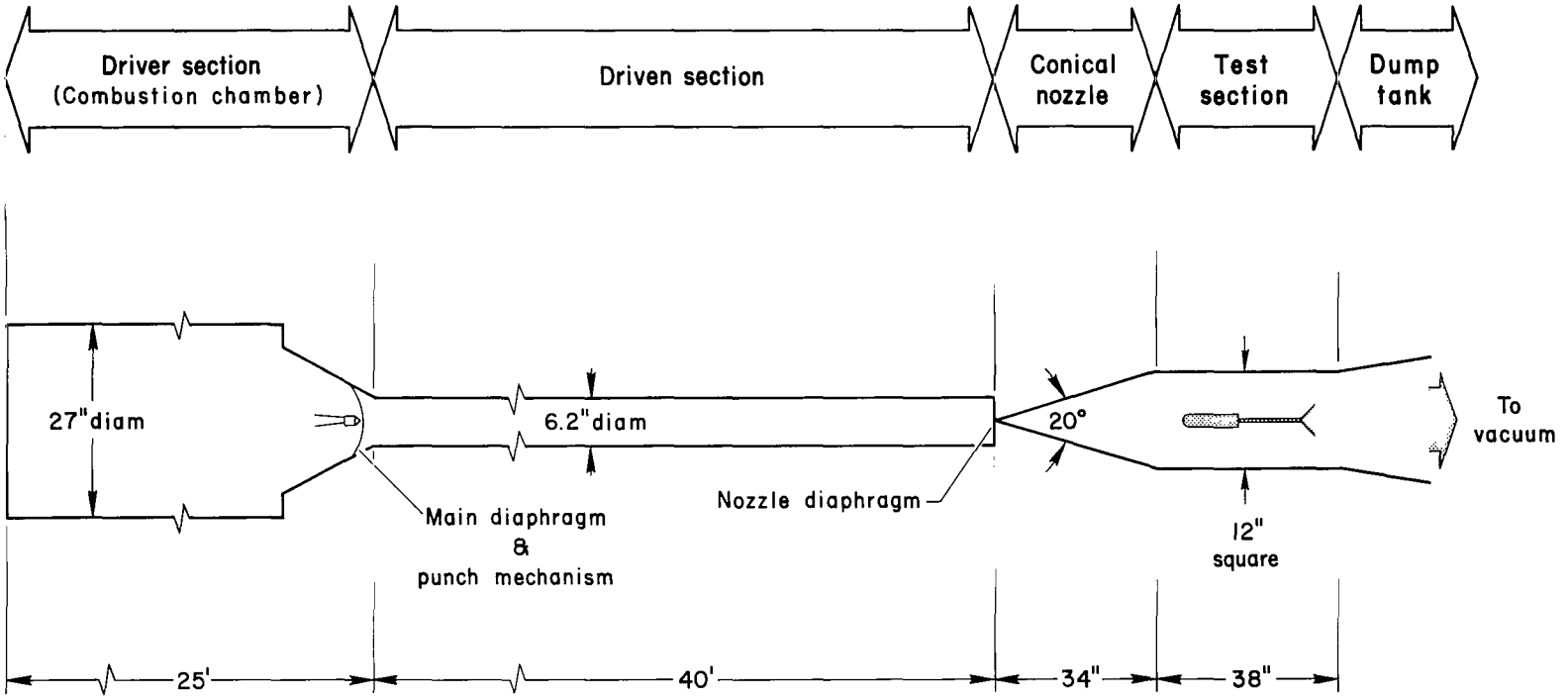

Figure 1.- Schematic drawing of Ames 1-Foot Shock Tunnel.

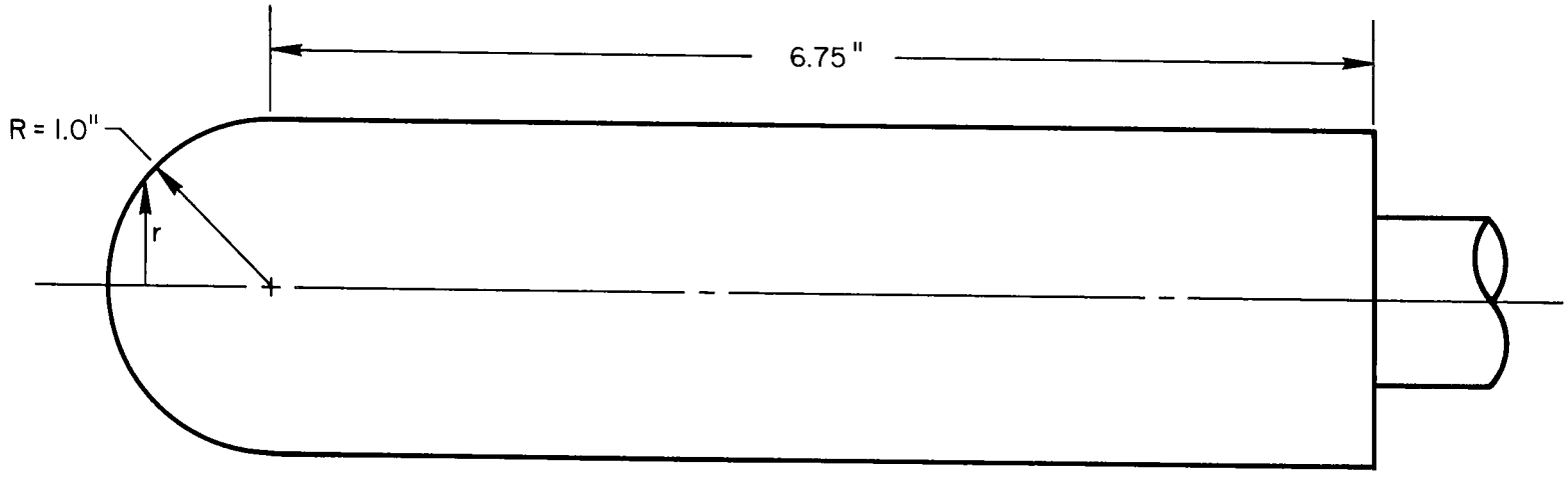

Configuration "A"

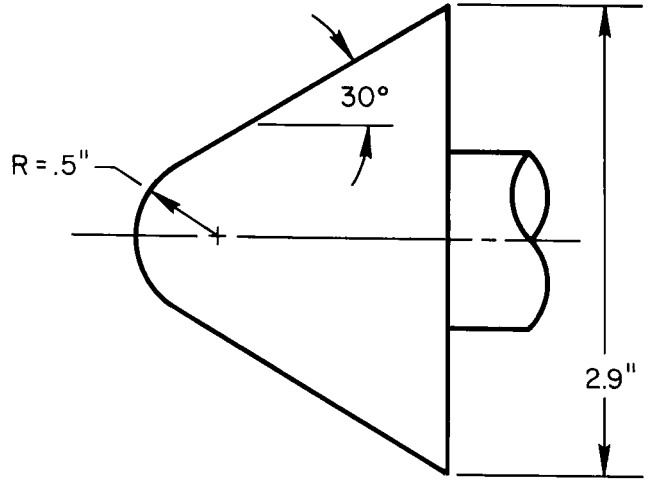

Configuration "B"

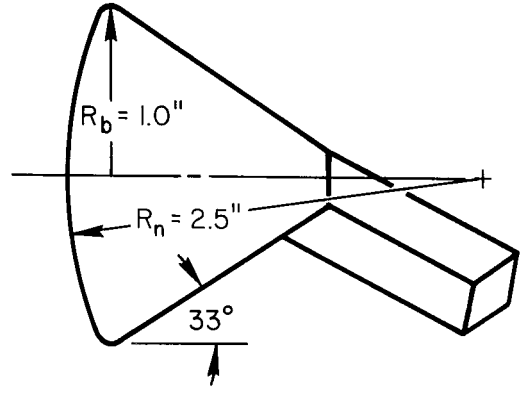

Configuration "C"

Figure 2.- Test models.

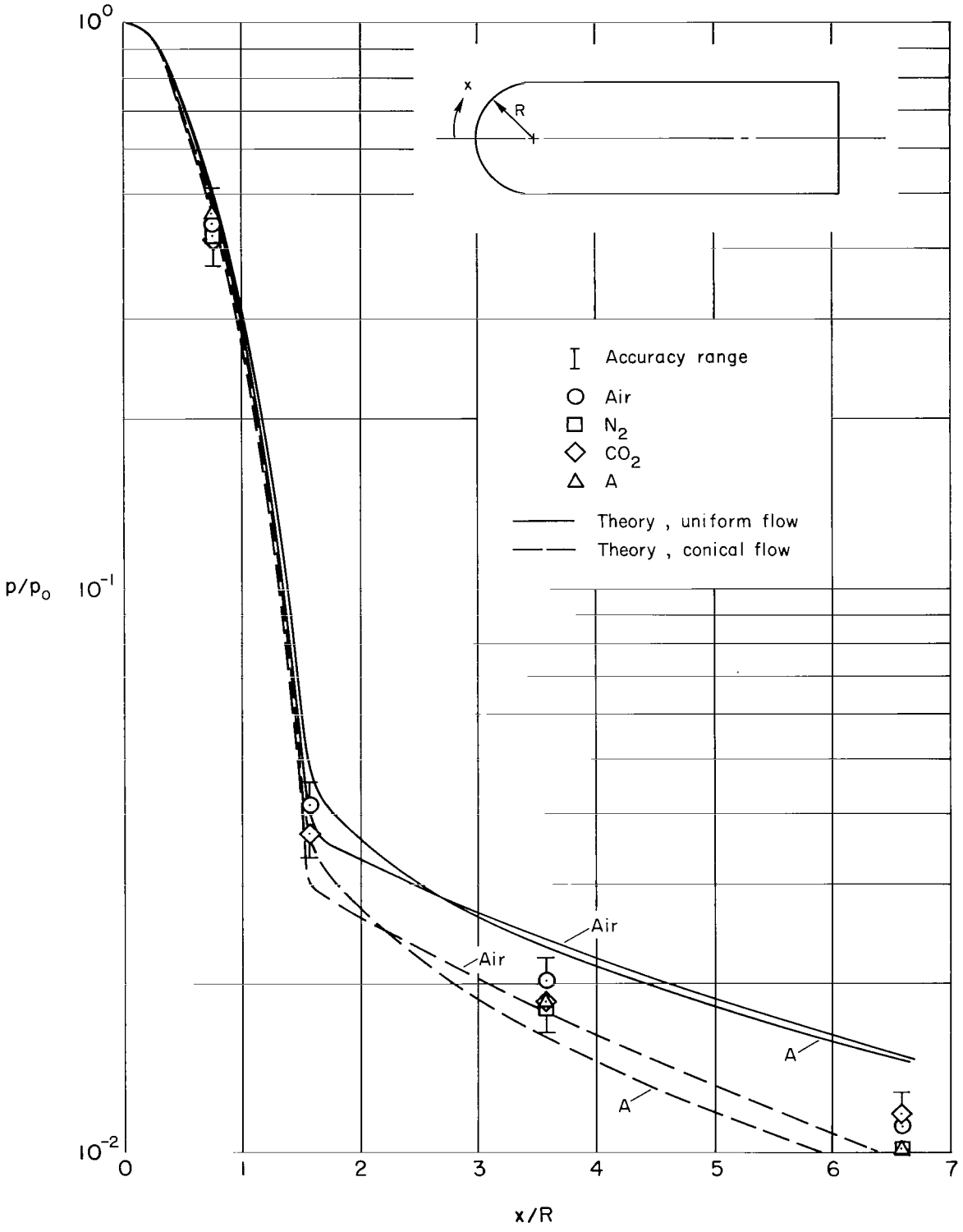

Figure 3.- Measured pressures on a hemisphere-cylinder for various gases.

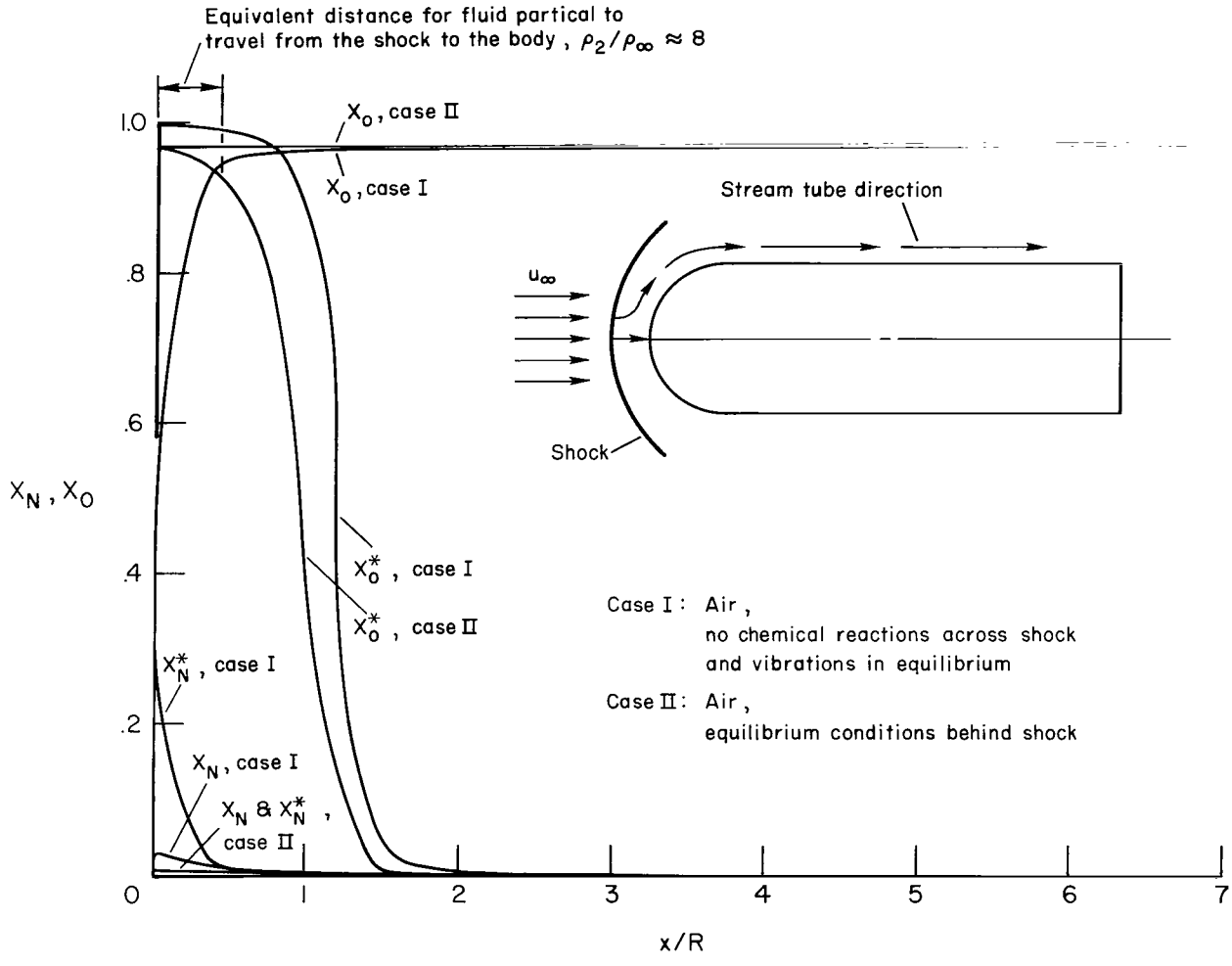

Figure 4.- Streamtube analysis for inferring the chemical state of the inviscid flow.

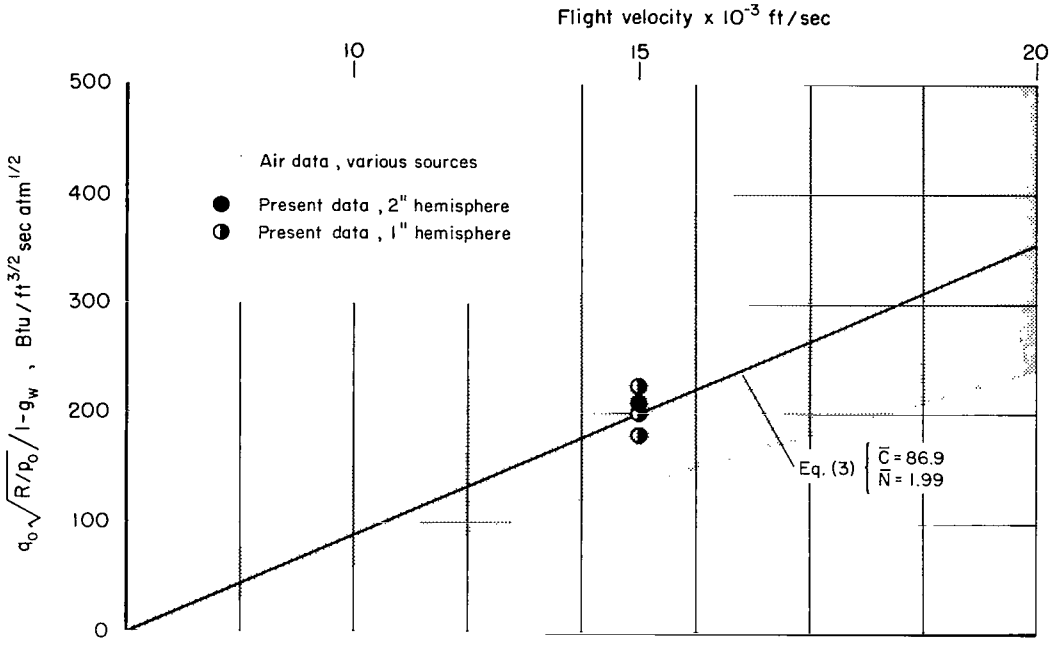

(a) Air.

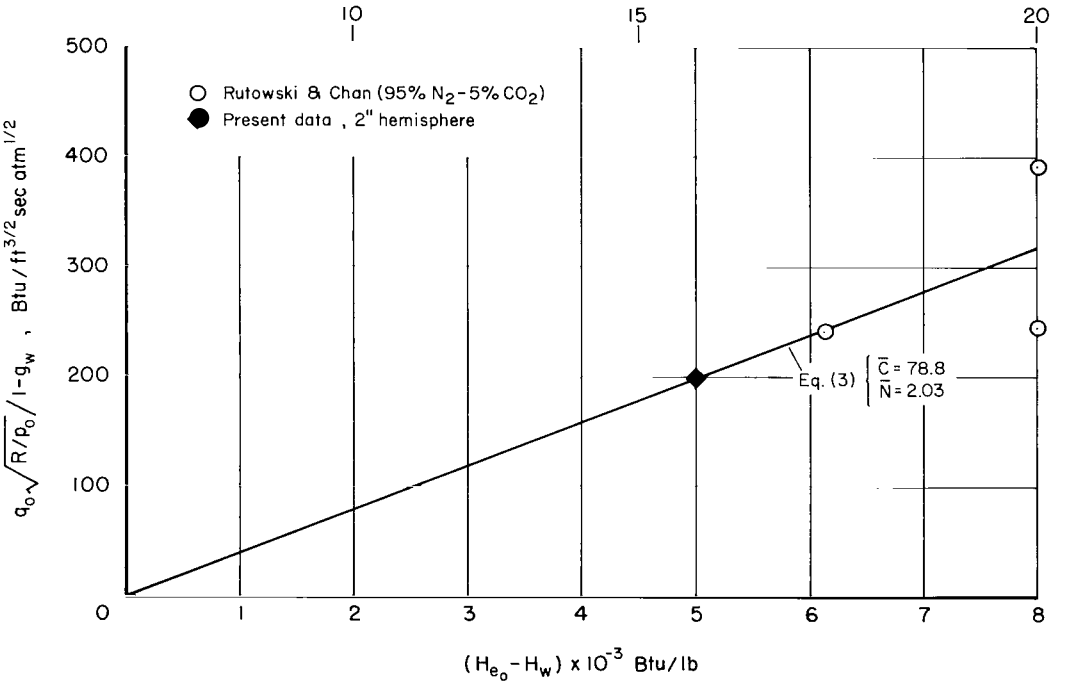

(b) Nitrogen.

Figure 5.- Comparison of stagnation-point heating with theory and shock-tube data.

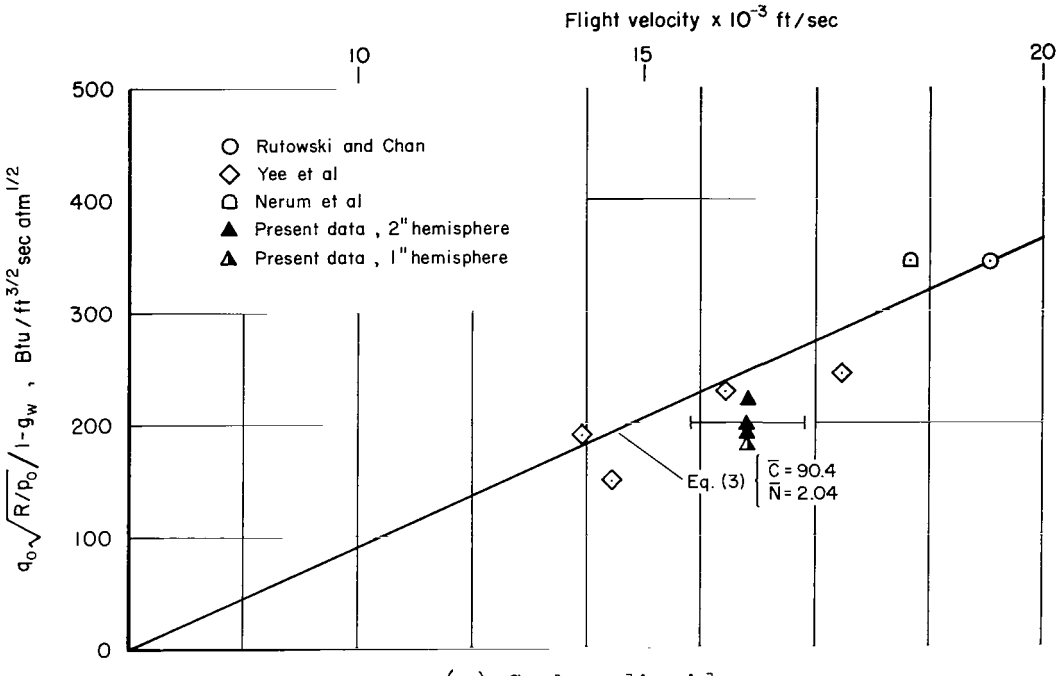

(c) Carbon dioxide.

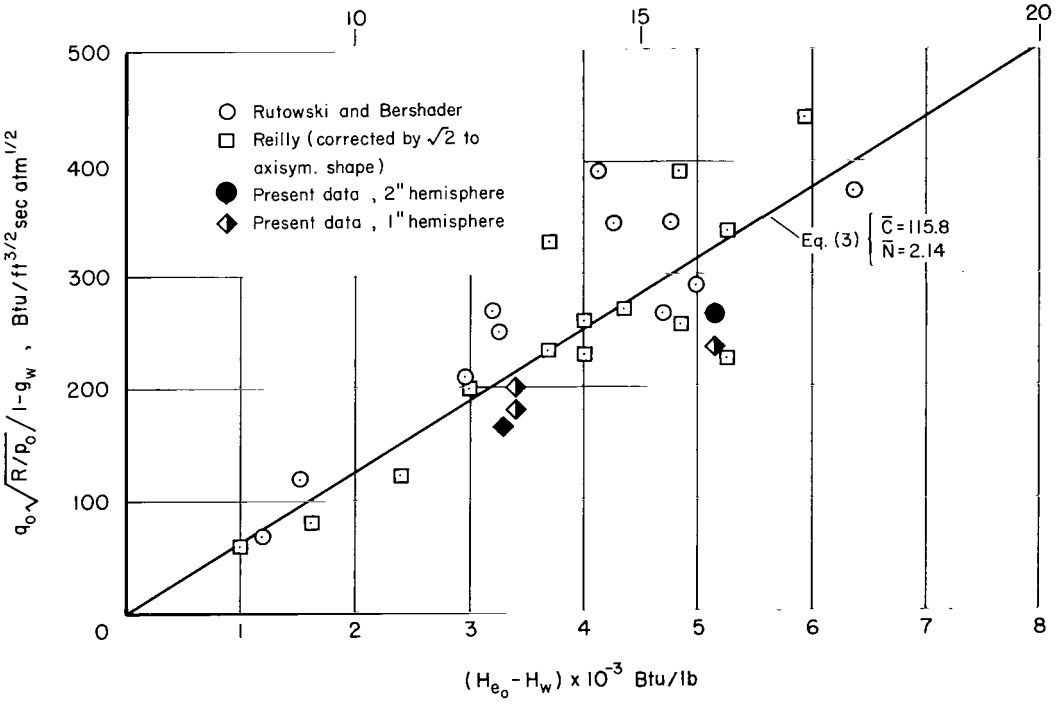

(d) Argon.

Figure 5.- Concluded.

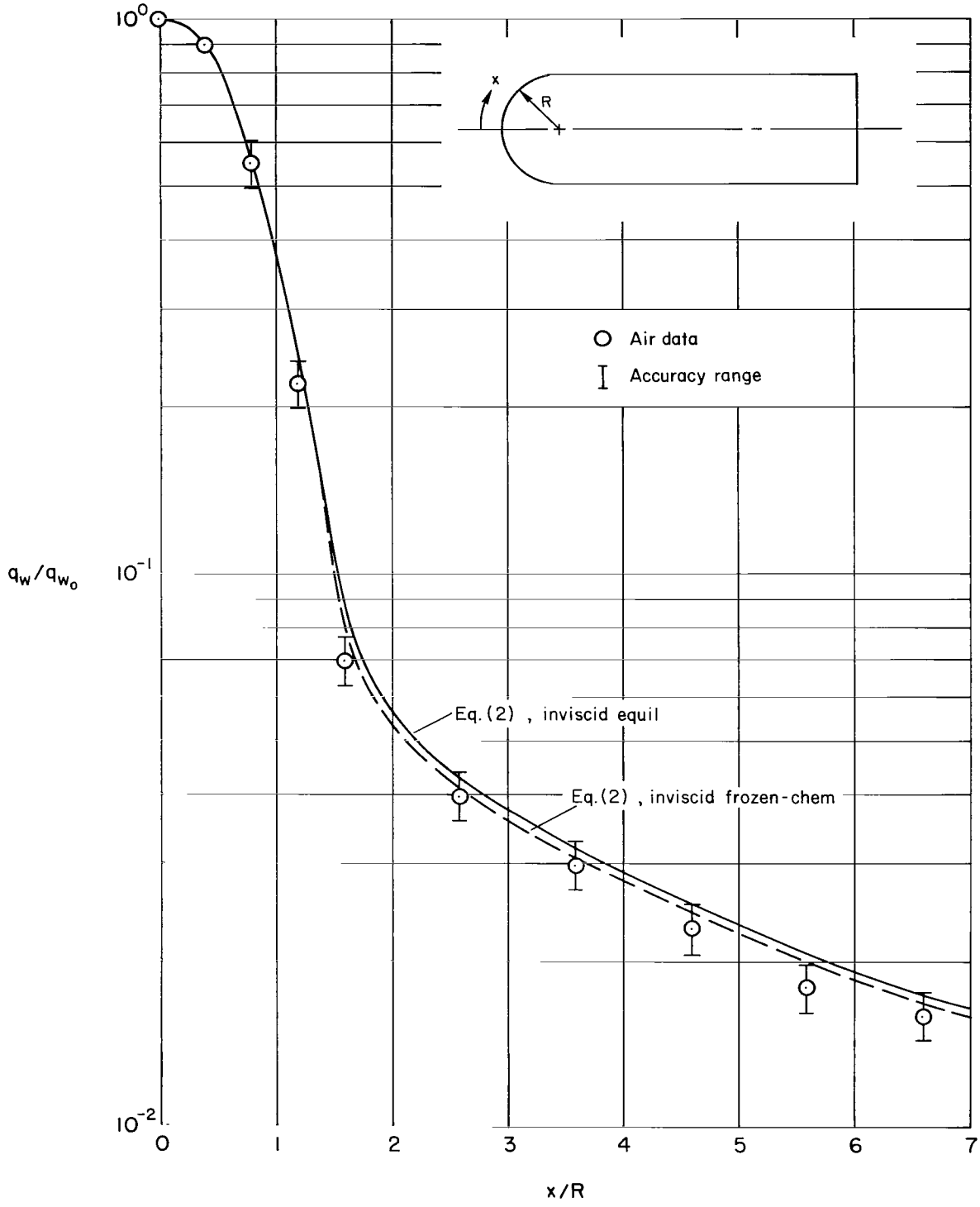

(a) Air.

Figure 6.- Heat-transfer distribution on a hemisphere-cylinder for various test gases.

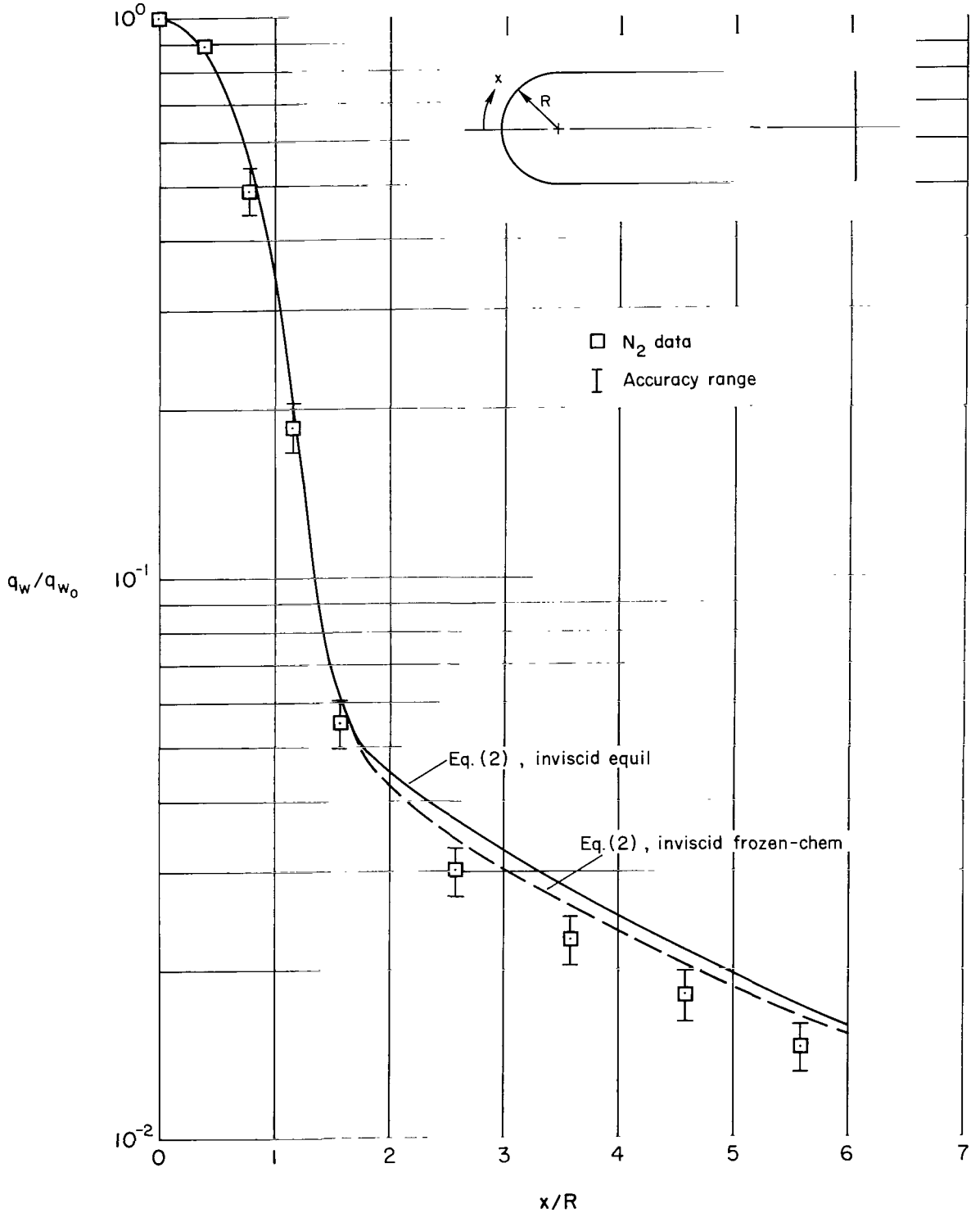

(b) Nitrogen.

Figure 6.- Continued.

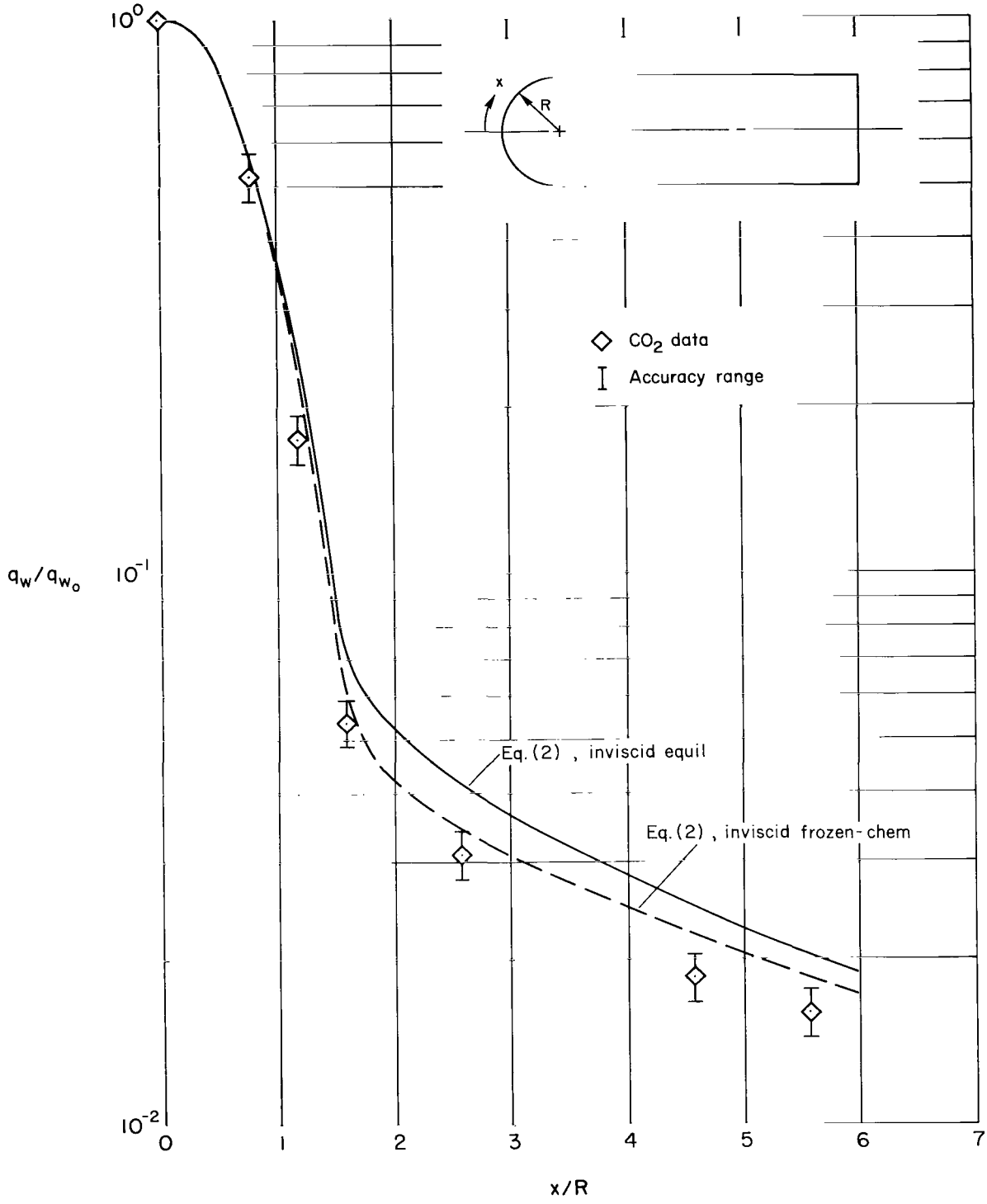

(c) Carbon dioxide.

Figure 6.- Continued.

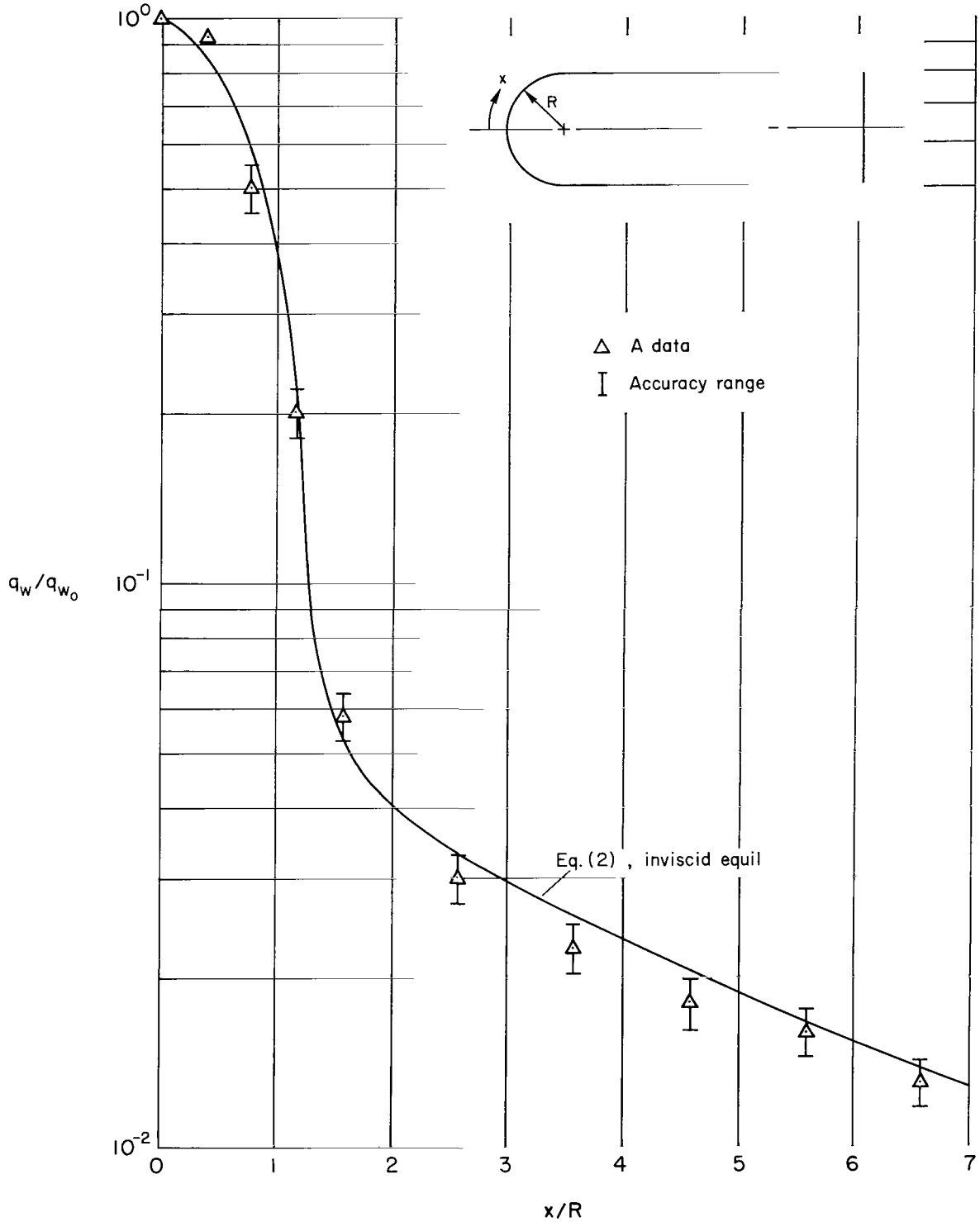

(d) Argon.

Figure 6.- Continued.

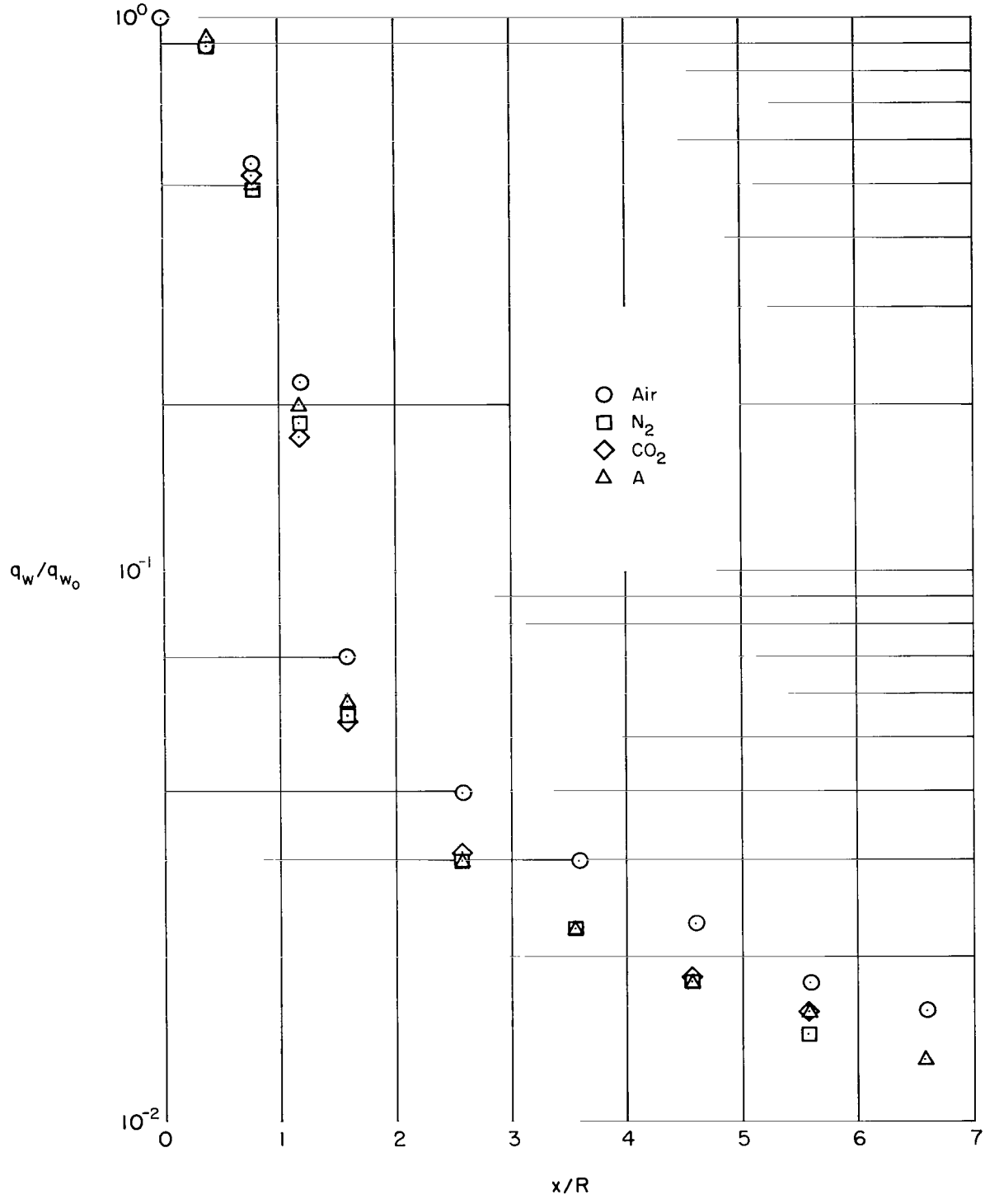

(e) Comparison of data for various gases.

Figure 6.- Concluded.

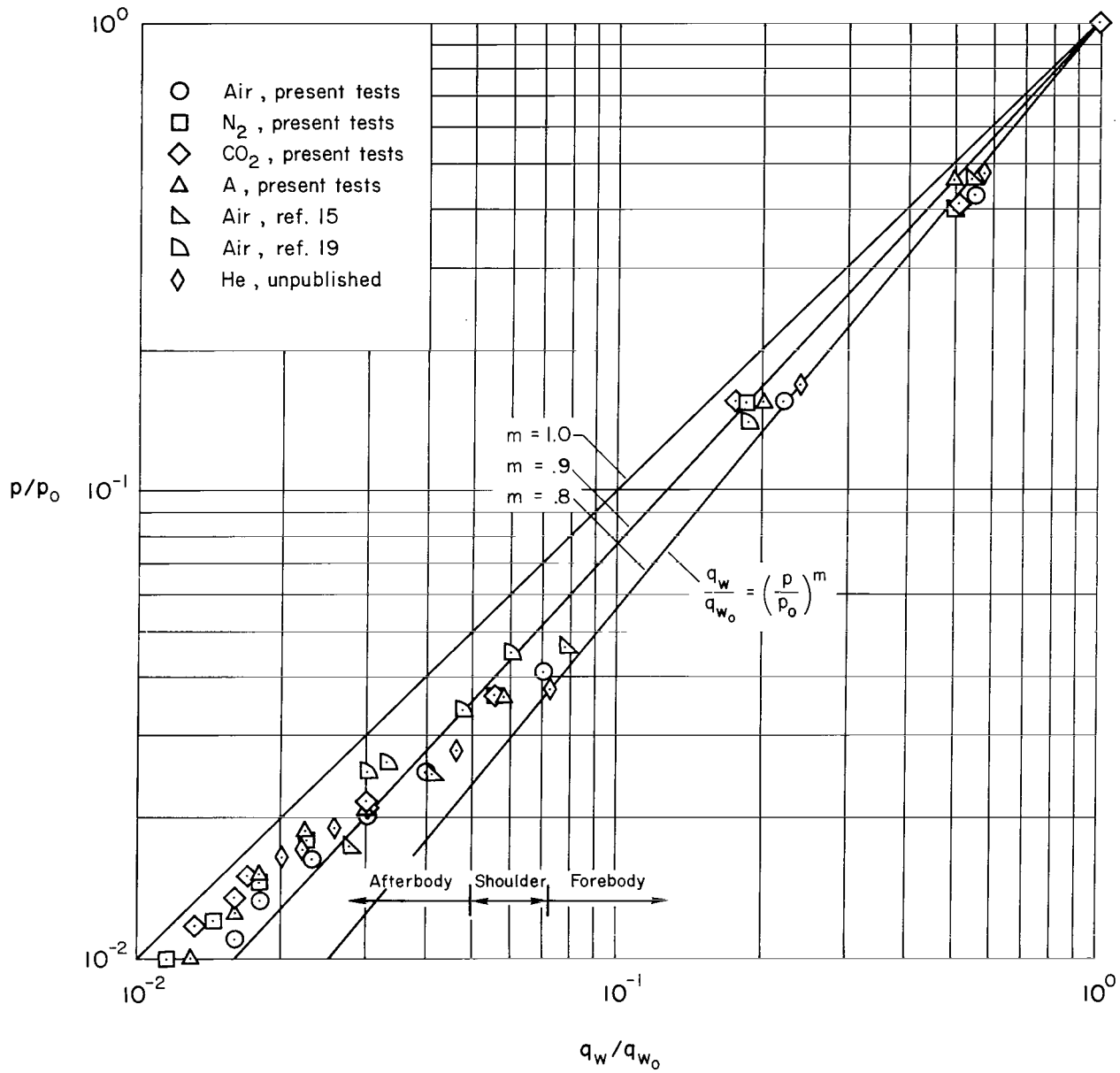

Figure 7.- Dependence of heating-rate ratio on pressure ratio for a hemisphere-cylinder in various test gases.

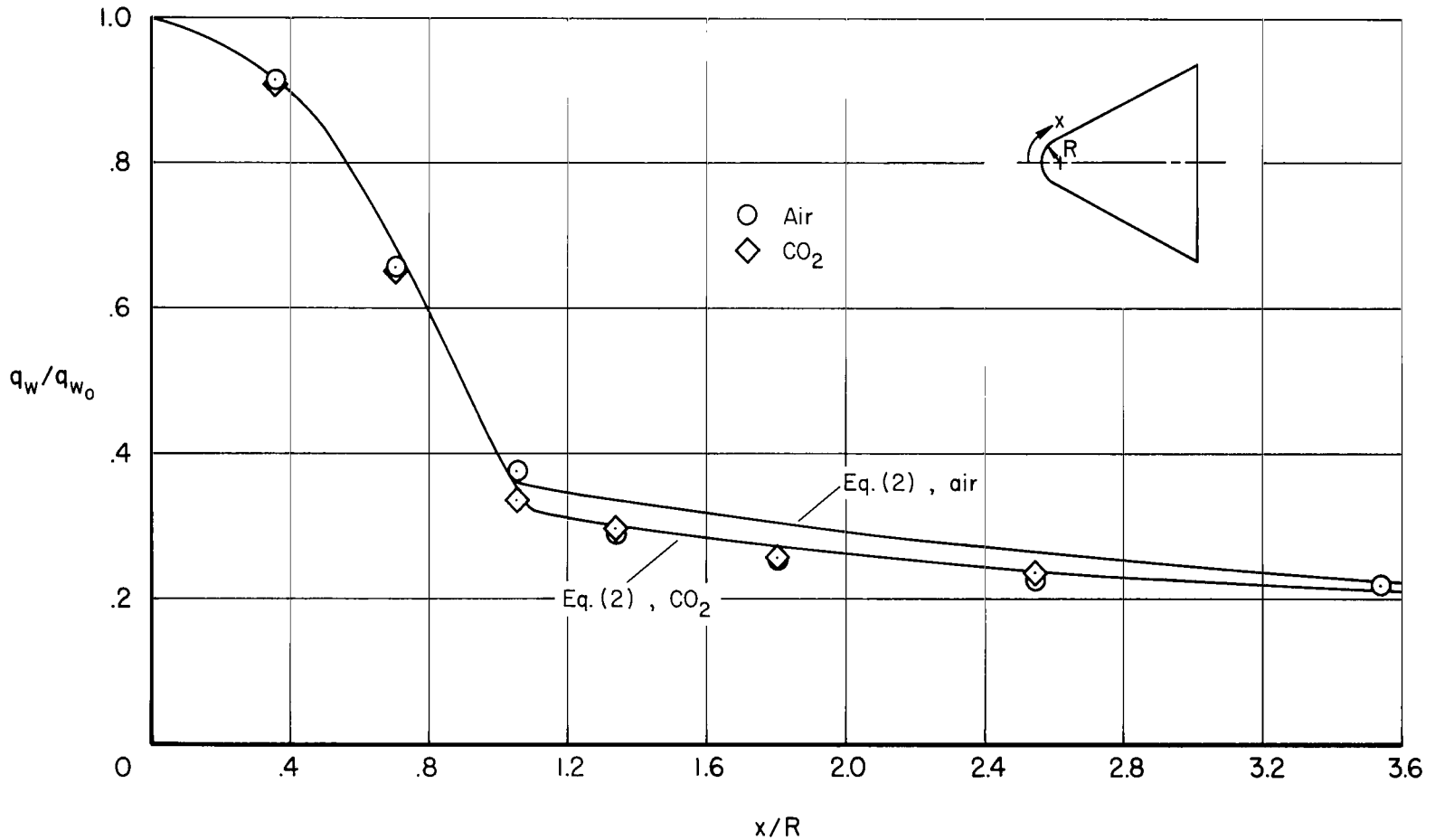

Figure 8.- Heating-rate distribution on blunted 30° cone in air and carbon dioxide.

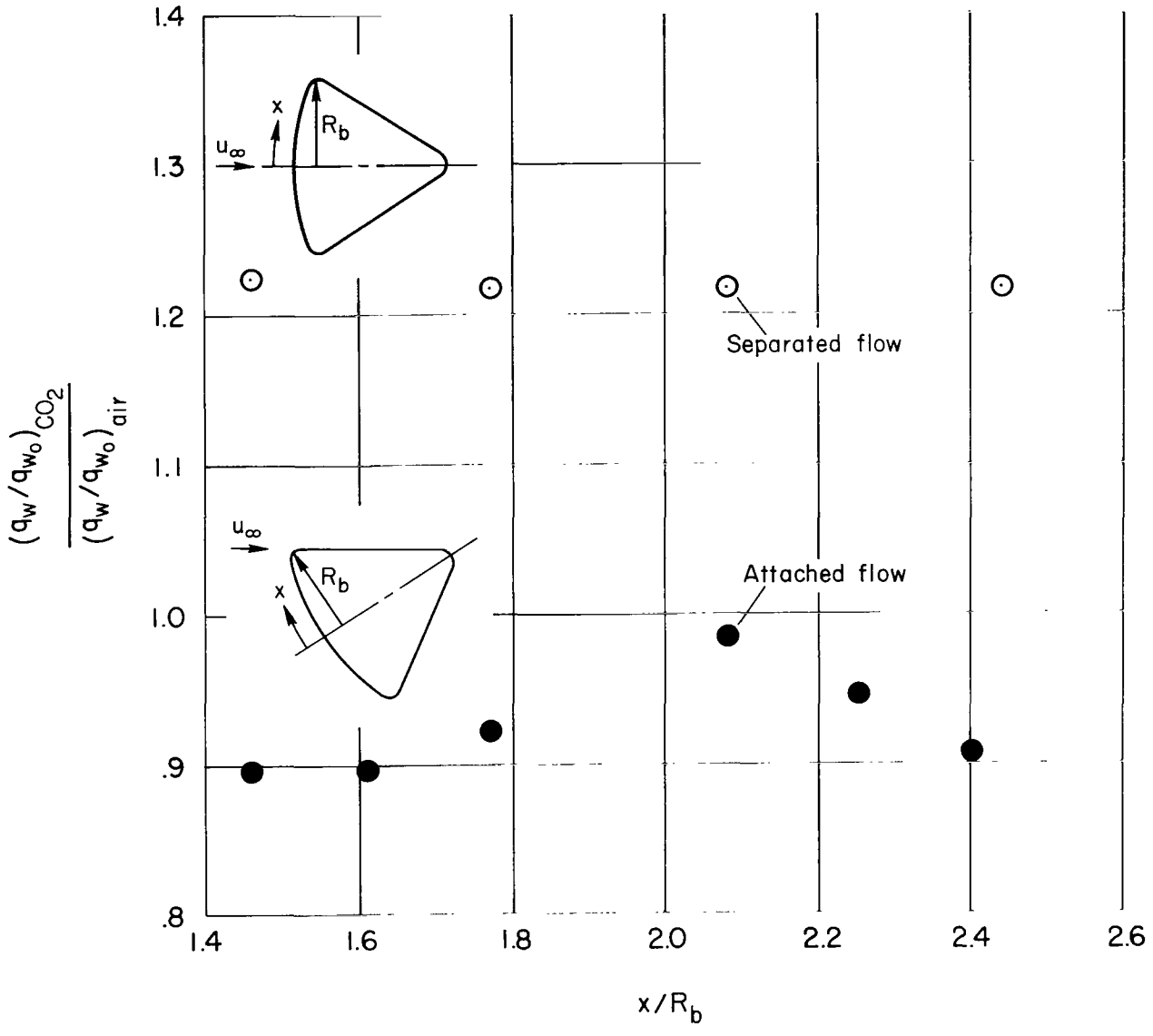

Figure 9.- Heating-rate distribution on capsule-type shape in air and carbon dioxide.

NASA-Langley, 1965 A-2156

3/18/62

"The aeronautical and space activities of the United States shall be conducted so as to contribute . . . to the expansion of human knowledge of phenomena in the atmosphere and space. The Administration shall provide for the widest practicable and appropriate dissemination of information concerning its activities and the results thereof."

—NATIONAL AERONAUTICS AND SPACE ACT OF 1958

NASA SCIENTIFIC AND TECHNICAL PUBLICATIONS

TECHNICAL REPORTS: Scientific and technical information considered important, complete, and a lasting contribution to existing knowledge.

TECHNICAL NOTES: Information less broad in scope but nevertheless of importance as a contribution to existing knowledge.

TECHNICAL MEMORANDUMS: Information receiving limited distribution because of preliminary data, security classification, or other reasons.

CONTRACTOR REPORTS: Technical information generated in connection with a NASA contract or grant and released under NASA auspices.

TECHNICAL TRANSLATIONS: Information published in a foreign language considered to merit NASA distribution in English.

TECHNICAL REPRINTS: Information derived from NASA activities and initially published in the form of journal articles.

SPECIAL PUBLICATIONS: Information derived from or of value to NASA activities but not necessarily reporting the results of individual NASA-programmed scientific efforts. Publications include conference proceedings, monographs, data compilations, handbooks, sourcebooks, and special bibliographies.

Details on the availability of these publications may be obtained from:

SCIENTIFIC AND TECHNICAL INFORMATION DIVISION

NATIONAL AERONAUTICS AND SPACE ADMINISTRATION

Washington, D.C. 20546